



## Article

# Understanding the Characteristics of Vertical Structures for Wind Speed Observations via Wind-LIDAR on Jeju Island

Dong-Won Yi , Hee-Wook Choi, Sang-Sam Lee  and Yong Hee Lee

Department of Research Applications, National Institute of Meteorological Sciences, Jeju 63568, Republic of Korea; wook2845@korea.kr (H.-W.C.); sangsam.lee@korea.kr (S.-S.L.); gonos2004@korea.kr (Y.H.L.)

\* Correspondence: dwyi@korea.kr

**Abstract:** Wind observations at multiple levels (40–200 m) have been conducted over a five-year time period (2016–2020) on Jeju Island of South Korea. This study aims to understand the vertical and temporal characteristics of the lower atmosphere. Jeju Island is a region located at mid-latitude and is affected by seasonal wind. The maximum wind speed occurs in the relatively lower altitudes during daytime and is delayed in the relatively higher altitude after sunset in a diurnal cycle. In the summer season, the altitudes appear earlier than in other seasons via the dominant solar radiation effect during daytime, and the altitude after sunset increases up to 160 m. However, the maximum wind speed in the winter season occurs irregularly among altitudes, and it is lower than that in the summer season. This can be attributed to the increase in the mean wind speed in the diurnal cycle caused by the strong northwestern wind in the winter season. These results imply that the relationship between near-surface and higher altitudes is primarily affected by solar radiation and seasonal winds. These results are expected to contribute to site selection criteria for wind farms.

**Keywords:** Wind-LIDAR; multiple-level winds; diurnal cycle; atmospheric boundary layer; maximum wind speed



**Citation:** Yi, D.-W.; Choi, H.-W.; Lee, S.-S.; Lee, Y.H. Understanding the Characteristics of Vertical Structures for Wind Speed Observations via Wind-LIDAR on Jeju Island. *Atmosphere* **2023**, *14*, 1260. <https://doi.org/10.3390/atmos14081260>

Academic Editors: Yubin Li and Jie Tang

Received: 12 July 2023

Revised: 7 August 2023

Accepted: 7 August 2023

Published: 8 August 2023



**Copyright:** © 2023 by the authors. Licensee MDPI, Basel, Switzerland. This article is an open access article distributed under the terms and conditions of the Creative Commons Attribution (CC BY) license (<https://creativecommons.org/licenses/by/4.0/>).

## 1. Introduction

With the acceleration of global warming, the demand for renewable energy sources that generate eco-friendly and clean energy, such as wind power, with reduced carbon emissions is gradually increasing [1–3]. Generally, wind-power-generating turbines are located within the surface layer (SL), which corresponds to ~10% of the lower layer of the atmospheric boundary layer (ABL); SL is further classified into inertial and roughness sublayers, which interact with the land surface [4]. Additionally, SL can be part of a thermally driven mixed layer (ML) and a nocturnal stable boundary layer (NL), which develop over daily diurnal cycle timeframes. During daytime, ML develops up to several kilometers owing to strong convection associated with solar radiation, whereas after sunset, with decreasing convection within ABL, ML is replaced by NL until sunrise. Concerning solar radiation, heat and momentum are exchanged within SL during daytime and nighttime, and these characteristics are also closely related to atmospheric movement and the calculation of wind power generation [5]. However, the processes occurring within ABL are still not properly understood [6,7]. Therefore, properly understanding the role of the lower atmospheric layer in wind power generation as a renewable energy source is crucial [8]. Additionally, although various studies have been conducted on the effect of the wind environment on wind power generation in lower atmospheric layers, including SL [9–12], long-term observations and research on vertical wind profile characteristics are insufficient.

Wind light detection and ranging (Wind-LIDAR) equipment is a state-of-the-art technology for obtaining wind measurements, and it has been developed rapidly over the decades following the invention of the laser in 1960 [13–21]. However, limitations, including a low spatial resolution and the inability to address local climate characteristics

that considerably impact wind peak and ramp predictions, still remain [22]. To overcome these limitations, ground-based remote observation equipment, such as Wind-LIDAR, was recently introduced for climate research [23]. Wind-LIDAR can remotely measure atmospheric winds and has a higher resolution than existing SODAR (Sonic Detection and Ranging) [24]. Although existing observation towers installed on the ground are limited in terms of height for wind resource estimation and vertical wind observation and require high installation costs, remote observation equipment such as Wind-LIDAR has advantages in that it is easy to move and install and is cost-effective; moreover, its height settings can be conveniently changed. In this context, the National Institute of Meteorological Sciences has conducted an intensive and long-term Wind-LIDAR observation at a point in the northern part of Jeju Island, which includes a section with an altitude of 40–200 m, where changes in SL can also be examined. The relevant observatory has been operated to select the location of wind power plants and evaluate the environment, which facilitates the provision of data for the analysis of vertical wind characteristics of the lower atmospheric layer, including SL, under the circumstance where long-term vertical observation data are rare. Therefore, this study intends to investigate the vertical structure and temporal variability characteristics of wind in the lower atmospheric layer, including SL, using long-term observation data on vertical wind. The sections of this paper consist of Section 2, which introduces data collected from observation equipment and analysis methods; Section 3, which presents monthly and daily variation characteristics of vertical wind; and Section 4, which includes the summary and discussion.

## 2. Data and Methods

The long-term vertical wind observations were conducted at the Bonggae (BG) Observatory in northern Jeju-si, Jeju-do, located at 351 m above sea level (Figure 1). The equipment used for the vertical wind observations was Wind-LIDAR (by Leosphere) ( $33.4621^{\circ}$  N,  $126.6289^{\circ}$  E), which is a technology applied in various fields to measure the distance to objects and speed using a laser and has been reported to be more reliable than conventional remote equipment such as SODAR [25]. In the surrounding environment where the observation equipment was installed, gentle slopes were generally spread out, and the surface roughness was 0.07 m, which is a value equivalent to the surface roughness class between 1.5 and 2 [26]; therefore, the influence of turbulence due to high obstacles was relatively small. The Wind-LIDAR has an observation altitude range from 40 m to 200 m, with 10 layers of vertical resolution at intervals of 10 m at altitudes of  $\leq 60$  m and 20 m at altitudes  $> 60$  m. The sampling rate was 1 Hz, and then the 10 min average time resolution was calculated for each wind direction and wind speed at all altitudes. Observations were conducted for approximately five years from September 2016 to July 2020, and quality control was applied according to the Meteorological Observations Standardized Manual [27]. A step test and the persistence test were performed on the collected data. Firstly, the step test was applied to exclude unrealistic wind, which shows a sudden change ( $10 \text{ ms}^{-1}$ ) in the 10 min average time resolution. Secondly, the persistence test examining the minimum change ( $0 \text{ ms}^{-1}$ , 0 degree) allowed for continuous time measurements (240 min). Subsequently, the hourly and monthly average values were calculated for the analysis of various time scales. Additionally, owing to the nature of optical sensor observation equipment such as Wind-LIDAR, incorrect measurements and missing data often result from atmospheric conditions. For example, clouds and aerosols affect backscatter, or the data collection rate decreases with an increasing altitude. Considering these factors, with 200 m, the altitude of the highest observation layer, as the standard, the days on which more than two-thirds of data were secured for 24 h a day were selected, and other days with a lower proportion of data were excluded from the analysis. The purpose of this study was to analyze the general vertical distribution characteristics of wind in the Bonggae area of Jeju Island using data collected over many years, which were averaged monthly and hourly according to the length of the analysis time. Additionally, considering the characteristics of the Korean Peninsula, which experiences all four seasons, we attempted to examine in

detail the diurnal characteristics of vertical winds by comparing the diurnal cycle for each season and mean value.

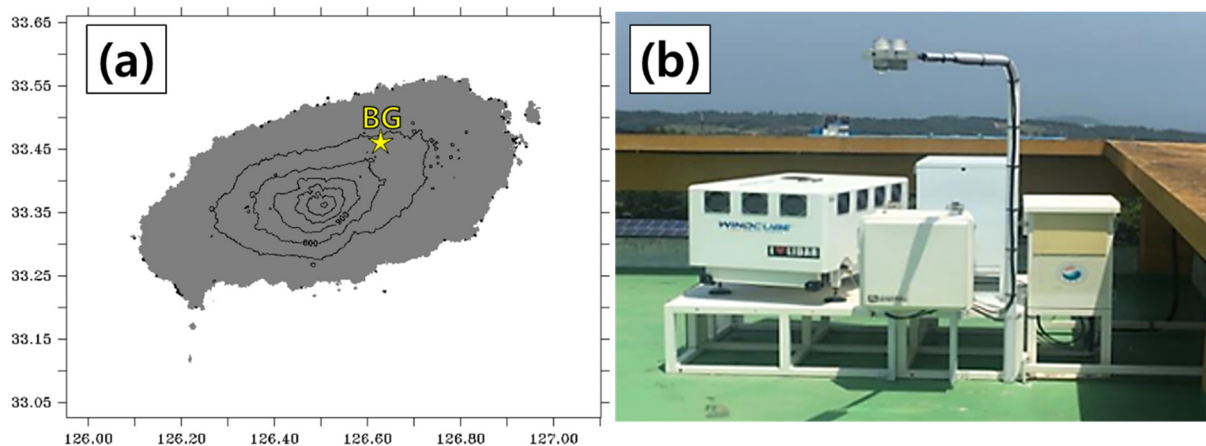


**Figure 1.** (a) Location (the yellow star symbol) and (b) Wind-LIDAR installation at Bonggae (BG) station on Jeju Island of South Korea.

### 3. Results

#### 3.1. Characteristics of Monthly Cycle and Characteristics via Elevation of Bonggae's Wind

The monthly mean wind speed for each altitude in the BG area varied over a range from  $2.57 \text{ ms}^{-1}$  to  $10.49 \text{ ms}^{-1}$ , and it showed an increase as the altitude increased (Figure 2). A typical vertical structure of the East Asian seasonal wind was shown, which is relatively weakened in summer and strengthened in winter. Based on years of observation, the average wind speed at altitudes of 40 to 200 m was found to be  $7.65 \text{ ms}^{-1}$  on average in the months of December, January, and February (DJF), which correspond to winter, and this was relatively larger than that in other seasons (March–April–May, MAM:  $6.66 \text{ ms}^{-1}$ , September–October–November, SON:  $6.21 \text{ ms}^{-1}$ ). Moreover, in the context of the wind direction, northwesterly wind was dominant relative to in other seasons (Figure 3). After winter, the northwest wind gradually weakened, and the wind speed gradually decreased; moreover, in spring (March to May), the northerly wind was dominant, and the westerly wind almost disappeared. In summer (June to August), the average wind speed was the weakest ( $4.79 \text{ ms}^{-1}$ ) of the year, and the easterly wind gradually increased. Subsequently, the easterly wind quickly changed its direction toward the westerly wind as the fall season (September to November) approached due to seasonal wind, followed by the arrival of the winter season.

As described earlier, the wind direction and wind speed in the BG area were highly correlated regardless of altitude, and when the wind was strong, the northwest wind was dominant, whereas when the wind was weak, the southeasterly wind dominated. Additionally, the characteristic of the clockwise circulation of the wind in all layers was confirmed during the year starting from spring. This means that wind directions at an altitude of 40–200 m have the same variability, suggesting that the influence of the surrounding seasonal winds, including in the observation area, plays a major role. Wind speed characteristics according to altitude were also clearly observed, with  $4.91$  to  $8.76 \text{ ms}^{-1}$  being noted in the highest layer of the observation altitude and  $3.76$  to  $6.96 \text{ ms}^{-1}$  being noted in the lowest layer of the observation altitude; moreover, the strongest wind speed occurred in the highest layer in December, and the weakest wind speed occurred in the lowest layer in July (Table 1). Thus, the monthly wind speed showed a distinct difference depending on the season in the vertical structure, and according to altitude, the upper layer was approximately 21.2–38.6% larger than the lower layer. In particular, the reason for the increase in the wind speed in the upper layer during winter is that the influence of ground friction decreases with an increasing altitude; moreover, the wind speed increases because it is influenced by the northwesterly seasonal wind. Additionally, the relatively

weak upper layer wind speed in summer is due to weakened horizontal advection as the vertical mixing between the upper and lower layers is strengthened by the ground being strongly heated by the sun along with the weakened northwest seasonal wind. Moreover, the wind direction associated with horizontal advection was also highly correlated with the wind speed, which could be clearly observed from the average wind speed for each wind direction in the order of north wind ( $11.0 \text{ ms}^{-1}$ ), west wind ( $7.2 \text{ ms}^{-1}$ ), east wind ( $6.0 \text{ ms}^{-1}$ ), and south wind ( $5.1 \text{ ms}^{-1}$ ).

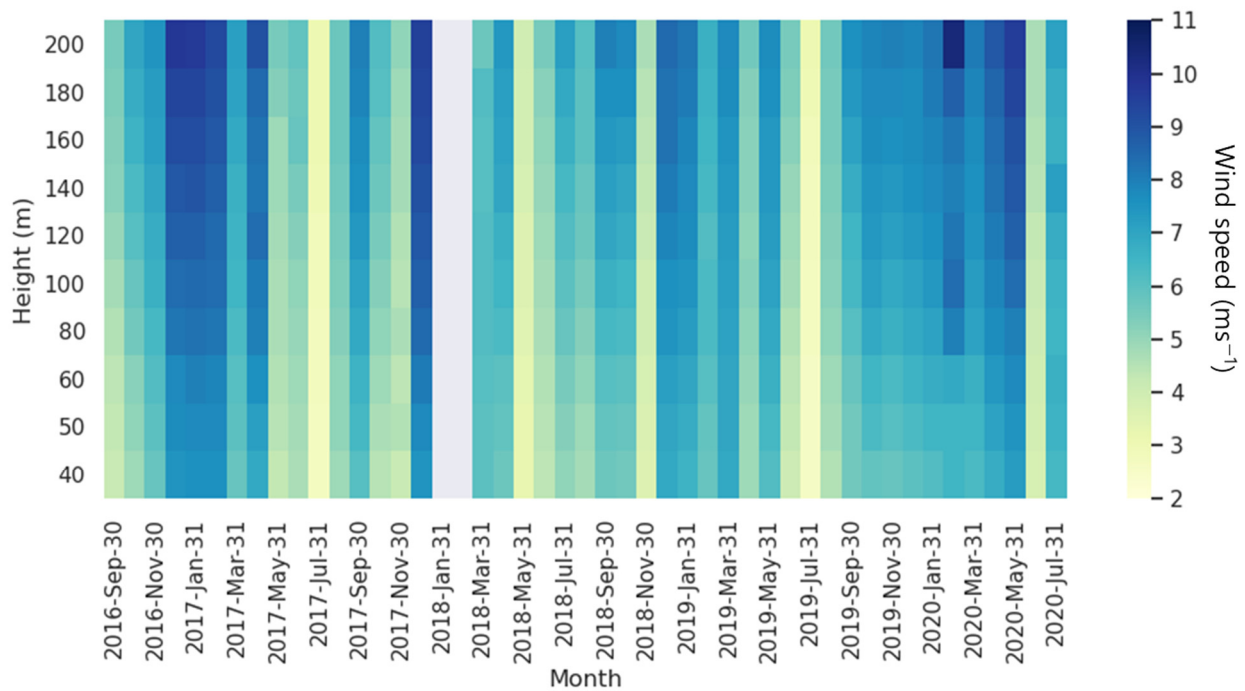


**Figure 2.** Monthly mean wind speed ( $\text{ms}^{-1}$ ) for vertical levels for Bonggae (BG) station. The shaded color in gray indicates the period of missing data (January 2018–February 2018).

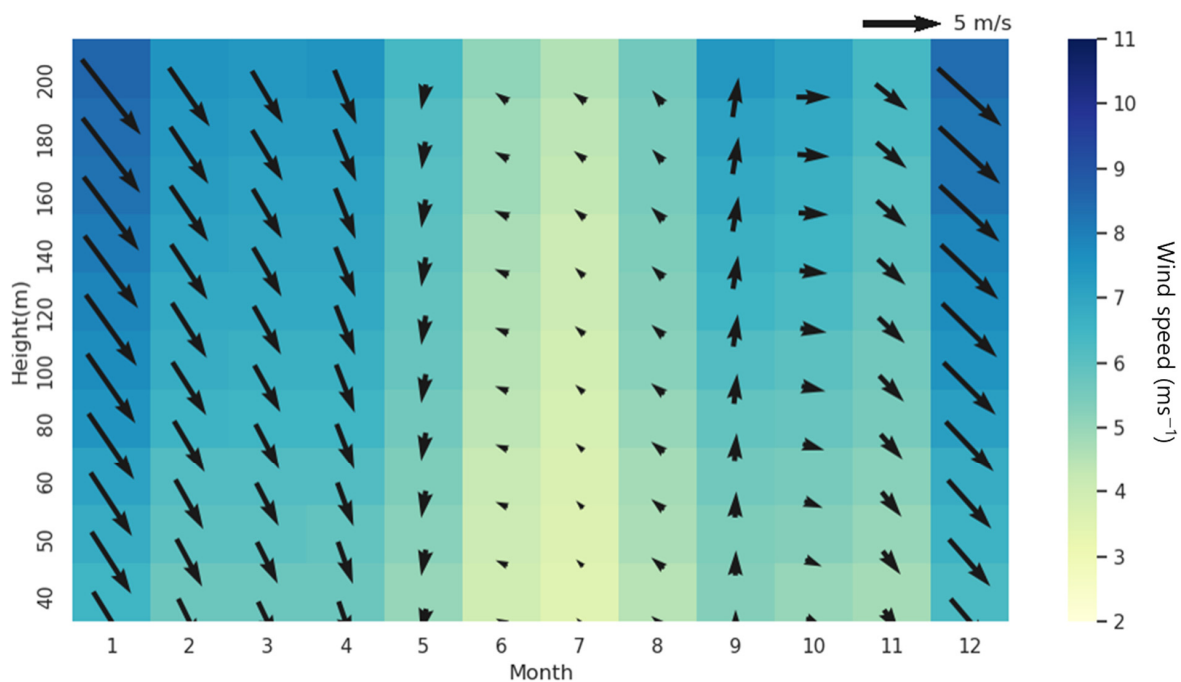


**Figure 3.** Monthly mean wind speed ( $\text{ms}^{-1}$ ) and wind direction for vertical levels.



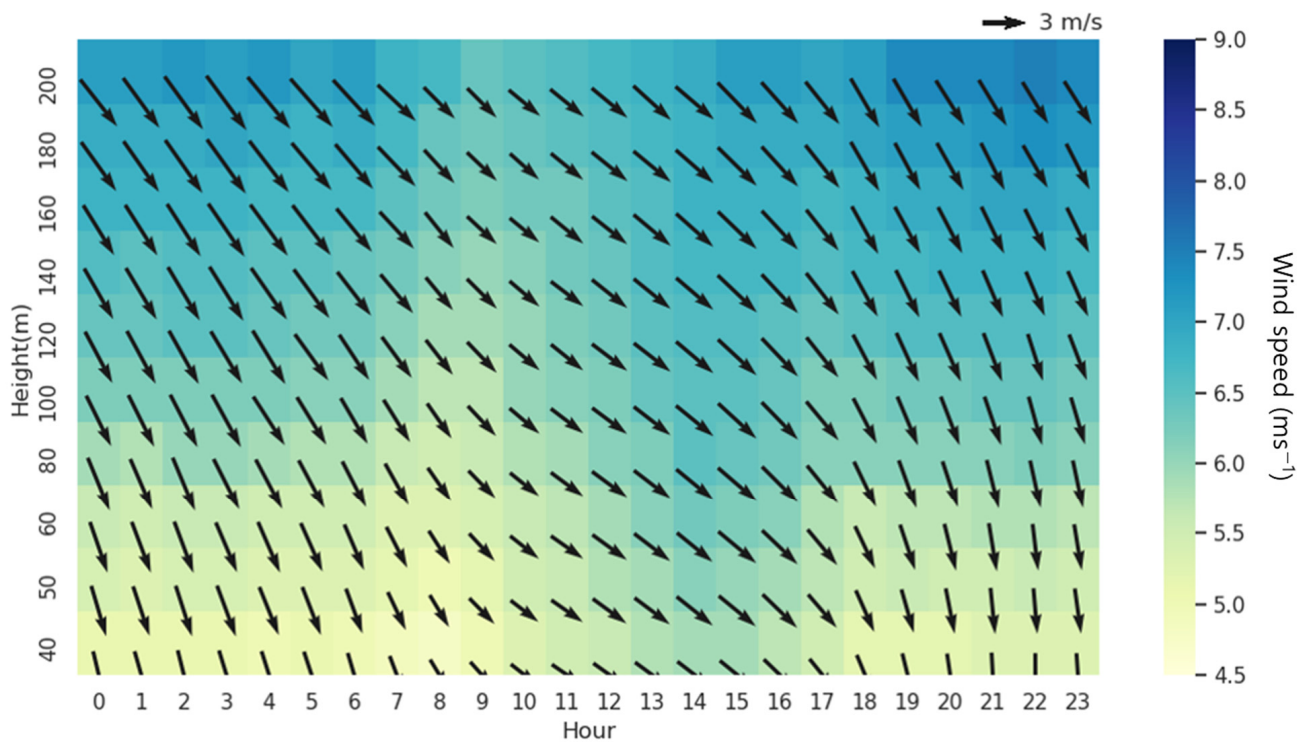


Figure 4. Diurnal cycle of mean wind speed ( $\text{ms}^{-1}$ ) and wind direction averaged for all periods.

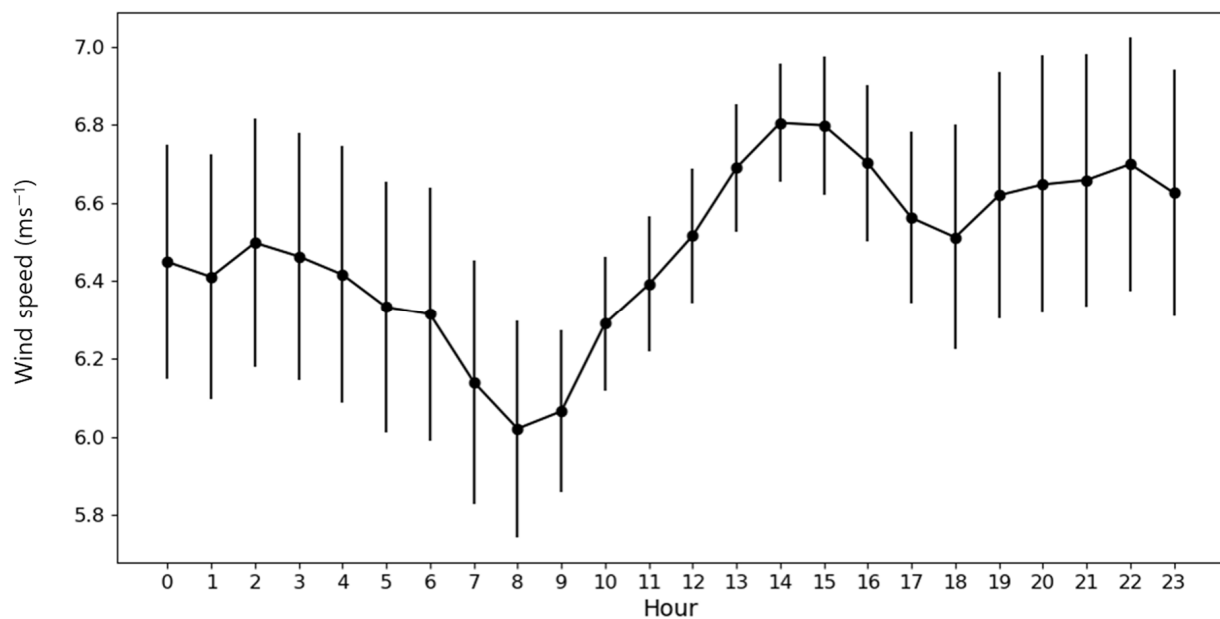


Figure 5. Diurnal mean and standard deviation of wind speed ( $\text{ms}^{-1}$ ) averaged for all altitudes.

### 3.3. Diurnal Characteristics in Each Season of Bonggae Winds

Earlier, the northwest wind was observed to dominate the monthly and daily cycles of the vertical wind, and the characteristics of the wind according to solar radiation were similar to each other (Figures 3 and 4). However, in the summer season (June–July–August, JJA), the strong westerly wind did not occur in a monthly cycle (Figure 3), unlike the diurnal cycle mean (Figure 4). This suggests that the diurnal cycle of the wind differs seasonally. To further investigate this variability, the seasonal characteristics of the diurnal cycle were examined; consequently, the main wind direction was different depending on the season (Figure 7), unlike the results of the year-round northwest wind dominating

the diurnal cycle mean during the entire period (Figure 4). The same as the average diurnal cycle result, winter was the season when the northwest wind was most dominant, meaning that winter is the most important season for the average annual wind direction in comparison with other seasons (Figure 7d). In winter, the biggest feature was that the northwest wind was continuously maintained regardless of altitude and the diurnal cycle. The northerly (westerly) wind in spring was weakened compared with winter by 29.4% (59.9%) (Figure 7a,d).

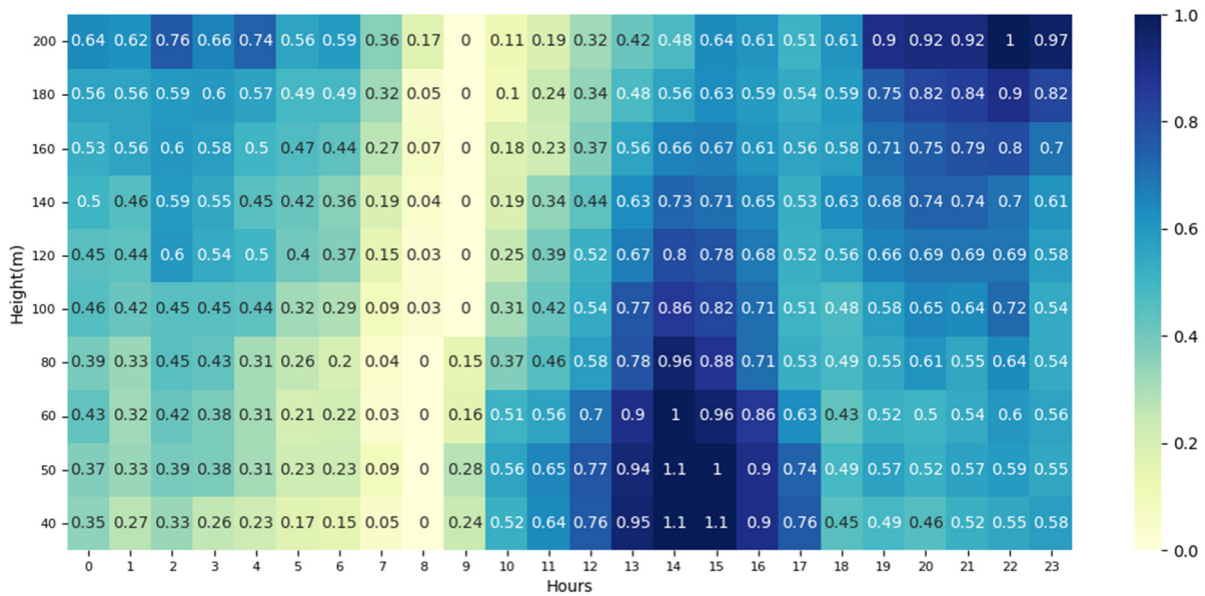


Figure 6. Difference between diurnal mean wind speed ( $\text{ms}^{-1}$ ) and minimum value for each altitude.

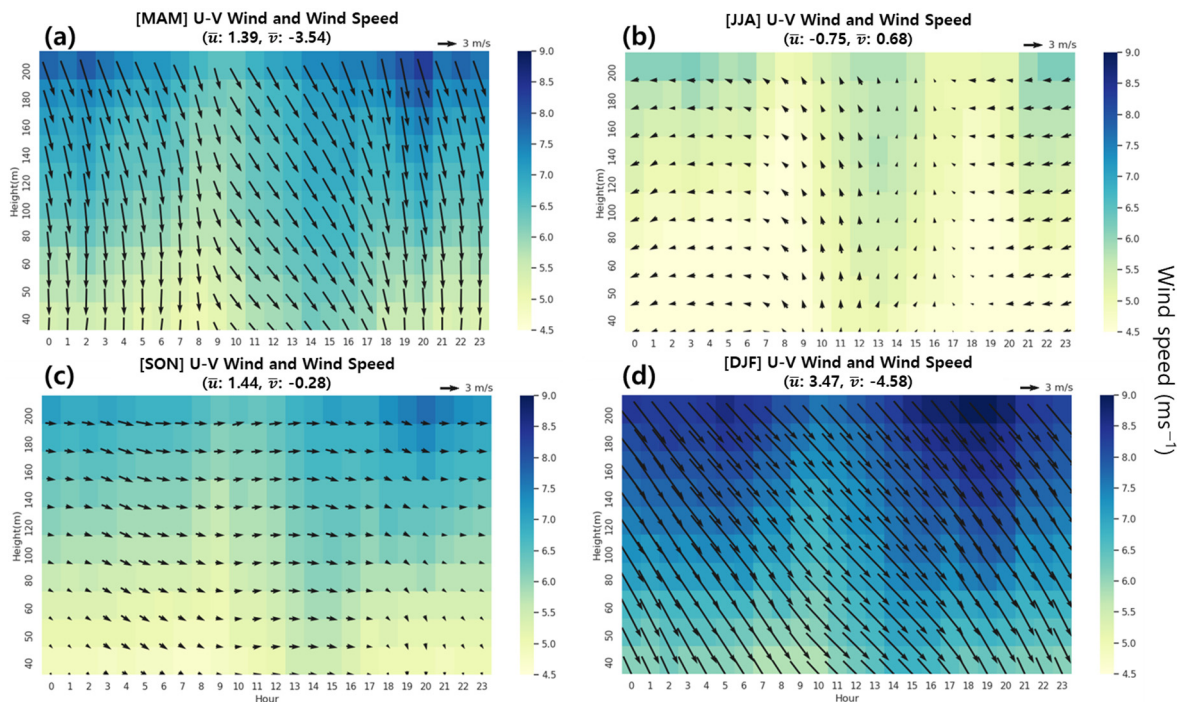
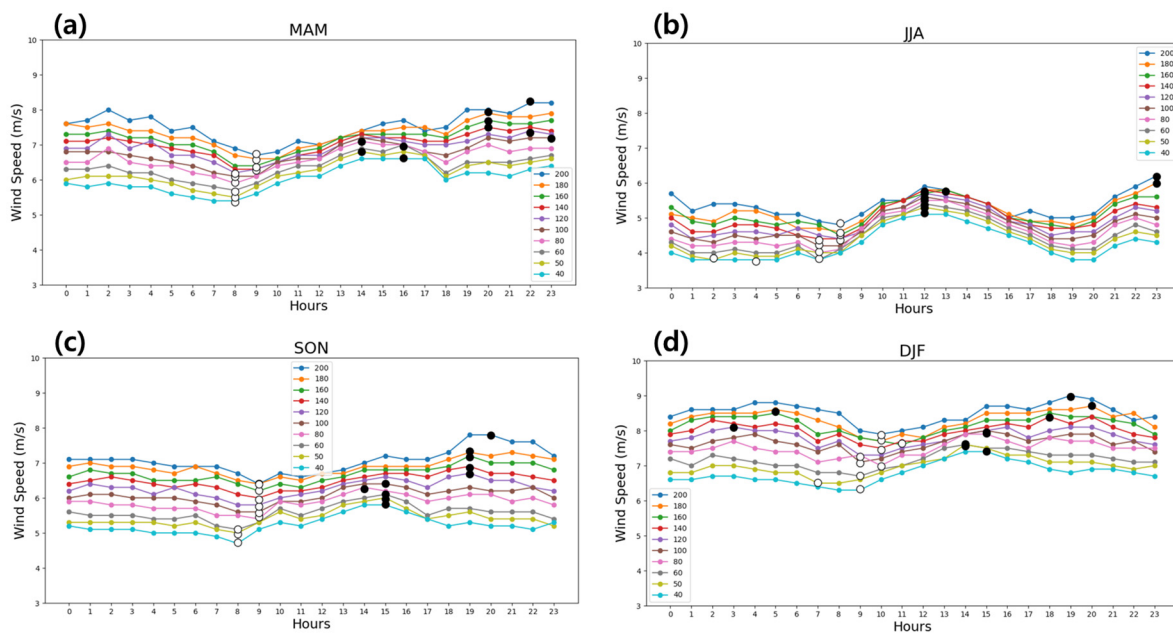


Figure 7. Diurnal cycle of mean wind speed ( $\text{ms}^{-1}$ ) and wind direction averaged for all periods for (a) March–April–May (MAM), (b) June–July–August (JJA), (c) September–October–November (SON), (d) December–January–February (DJF). Note that the values of  $\bar{u}$  and  $\bar{v}$  are averaged for all altitudes and time from u-component and v-component.

During the summer, the strong northerly wind switched to a southerly wind because of seasonal wind changes (Figure 7a,b). This phenomenon occurred because of the topographic effect, as the observation site is located on the downwind side from Hallasan (Mt. Halla, 1947 m), which blocks southerly wind during the summer (Figure 1a). And the influence of horizontal advection flow decreased due to strong vertical mixing caused by solar radiation in summer. Then, the wind direction changed from easterly to westerly in fall, unlike in summer (Figure 7b,c). Subsequently, the northwesterly wind reached its peak strength in winter because of seasonal wind changes. And it could also be enhanced by a reduced topographic effect, as the observation site is located on the upwind side from the mountain in winter. The results demonstrate that the wind in the Bonggae area of Jeju shows different characteristics according to the season.

### 3.4. Maximum Wind Speed Characteristics of Bonggae Wind According to Altitude

Previously, we found that the minimum wind speed at each altitude occurred at 8 to 9 a.m. on average and was delayed by ~1 h in the upper layer compared with the lower layer (Figure 6). The wind speeds at each altitude were confirmed to be closely related to each other, exhibiting similar variability between adjacent altitudes. However, the correlation of wind speeds at adjacent altitudes weakened as the altitudes were gradually separated farther (Table 2), suggesting that the time lag at each altitude may occur differently. The diurnal wind speed was minimal at 8–9 a.m. on average, and its strength gradually increased as a result of increased vertical mixing owing to ground heating after sunrise. The time when the maximum wind speed was observed, unlike the minimum wind speed, was considerably influenced by monsoonal winds and ground heating by the sun in each season. To examine this phenomenon of the vertical structure in detail, the time of day when the wind speed was maximized at each altitude was compared and analyzed according to season (Figure 8).



**Figure 8.** Diurnal mean wind speed ( $\text{ms}^{-1}$ ) for vertical levels for (a) March–April–May (MAM), (b) June–July–August (JJA), (c) September–October–November (SON), (d) December–January–February (DJF). The black (white) filled dots indicate the value when the maximum (minimum) wind speed occurred for each level.

A common feature of all seasons was that the maximum wind speed occurred first in the lowest layer after sunrise, and then the maximum wind speed occurred in the upper layer. However, there was a difference in the occurrence of the delayed maximum wind



speed depending on the season. The occurrence of the maximum spring wind speed could be largely divided into two groups: the first occurred at 2–4 p.m. in the section at an altitude of 40–80 m, which was approximately half of the lower layer of the observed altitude, and then the second, delayed by 4 h, occurred at 8–11 p.m. in the section at a relatively high altitude of 100–200 m (Figure 8a). As mentioned earlier, the fact that the maximum wind speed at each altitude occurs at different time points means that the wind speed at each altitude is determined differently. In the lower altitude, the wind speed gradually increased after sunrise to reach the maximum at ~3 p.m., and then it decreased with decreasing vertical mixing. However, in the higher altitude with relatively strong wind, the wind speed that decreased after sunrise gradually increased again and continued to increase, even after sunset, which resulted in the maximum wind speed occurring at night. The maximum wind speed in spring exhibited a time lag between the different altitudes owing to vertical mixing associated with the diurnal cycle of solar radiation. The fall also showed similar results to the spring, with the maximum wind speed occurring at 40–100 m in the lower layer at approximately 2–3 p.m. and then at 120–200 m at 7–8 p.m., delayed by 4 h (Figure 8c).

The summer showed considerably different results from the previous two seasons; basically, the average wind speed was relatively small at all times, and the variability among altitudes was also the smallest (Figure 8b). In particular, the variability among altitudes was minimal at ~11 a.m. after sunrise, and the maximum wind speed occurred in all sections of 40–160 m, except for the top two layers at 12 a.m.–1 p.m. Thus, the relatively small diurnal variability of the wind speed in summer compared with other seasons and the occurrence of the maximum wind speed were almost simultaneously correlated with vertical mixing caused by overwhelmingly strong solar radiation. Consequently, the occurrence of the maximum wind speed in the higher altitude was also delayed by 10 h in the 180–200 m section. However, in winter, the average wind speed was relatively higher than that in other seasons, unlike summer, and the biggest feature was the time when the maximum wind speed appeared to be distributed at various times (Figure 8d). Although the maximum wind speed first occurred in the 40–100 m section at 2–3 p.m. after sunrise, nonlinear characteristics appeared regardless of delay, such as at 6 p.m., 7 p.m., and 8 p.m., and at 3 a.m. and 5 a.m., at higher altitudes. This was mainly due to the influence of the northwest seasonal wind, which becomes stronger in winter, rather than the influence of solar radiation. Additionally, these characteristics appeared similarly in the hours of day when the minimum wind speed at each altitude occurred, with a constant delay of ~1 h between the upper and lower layers in spring and autumn, a long delay of ~6 h in summer, and some delay in winter, but with irregularities among altitudes.

### 3.5. Long-Term Tendency of Bonggae's Wind

From the results of the approximately five-year observation in Bonggae, we found that the wind speed exhibited an increasing tendency (Figure 9). The wind speed data from four adjacent automated weather station (AWS) points (Table 3) were compared to confirm whether these characteristics were limited to one area, and the same increasing trend was also observed. Nevertheless, because the tendency in this long period from a climatic perspective may be a natural variability, the AWS analysis period was extended back to the year 2000 to examine wind speed variability for a total of 20 years (Figure 10). Though there was an increase or decrease depending on the year, the wind speed had been steadily decreasing from about 2004 to 2016, and these results have also been presented in a global trend analysis using the Coupled Model Intercomparison Project (CMIP6) [28] and East Asian studies using observation data [29–32]. Since then, though there have been differences in time depending on the analysis area, the wind speed changed again around 2016 [31,32] (Liu et al., 2018; Kim and Paik., 2015), which is consistent with the results at Bonggae and AWS. This means that properly understanding the long-term tendency of wind speeds not only for location selection and the power generation calculation of wind power generation complexes but also for their long-term operation is crucial [33–36].

Furthermore, expanding observations and operations using Wind-LIDAR to a wider area in the future is essential.

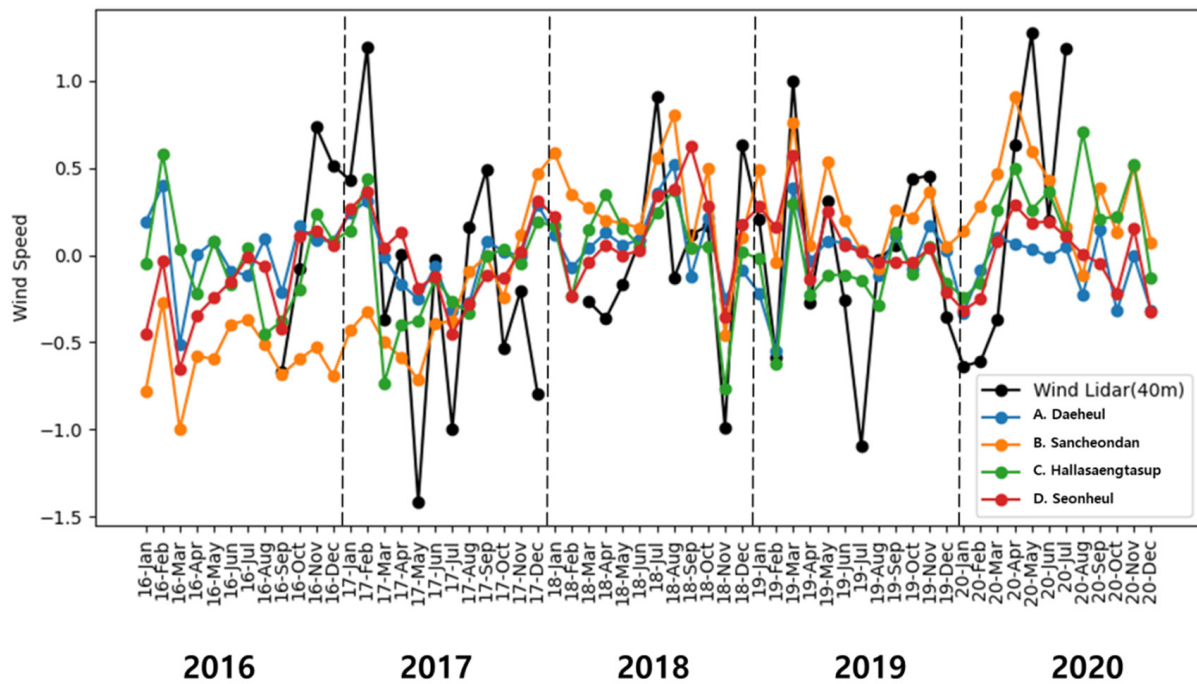


Figure 9. Monthly variability of wind speed ( $\text{ms}^{-1}$ ) for Wind-LIDAR at 40 m at BG station and AWSs around BG station.

Table 3. Basic information of automated weather stations around BG station.

#	Name	Latitude ( $^{\circ}\text{N}$ )	Longitude ( $^{\circ}\text{E}$ )
A	Daeheul	33.447336	126.56546
B	Sancheondan	33.50081	126.64947
C	Hallasaengtasup	33.43023	126.59777
D	Seonheul	33.48209	126.70904

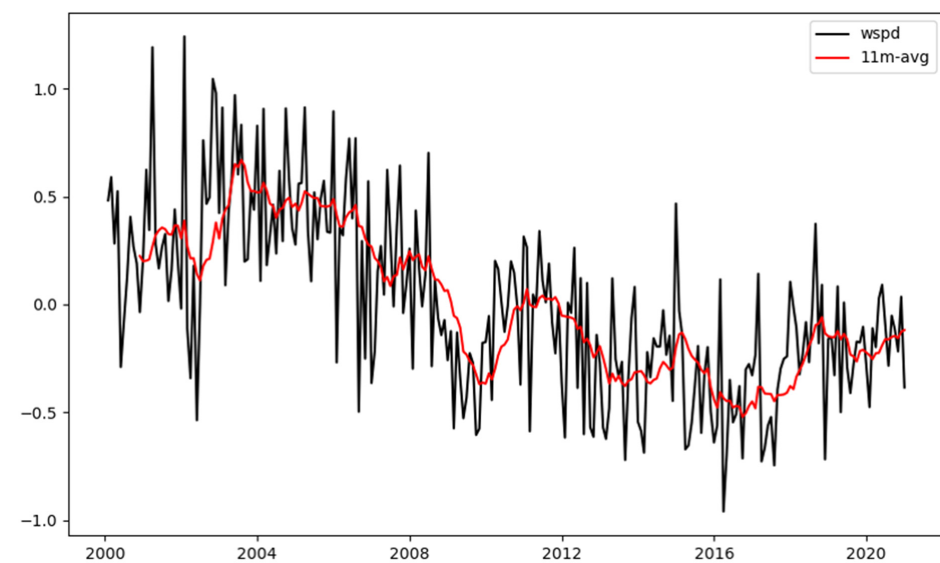


Figure 10. Monthly variability of wind speed ( $\text{ms}^{-1}$ ) averaged for AWSs around BG station. The red line indicates 11-month running mean.

#### 4. Summary and Discussion

Herein, we investigated the characteristics of vertical winds for the monthly and diurnal cycles at the lower layer (40–200 m) of ABL in the Bonggae area of Jeju Island. For the monthly cycle, the wind speed weakened/strengthened in summer/winter, and the wind direction was dominated by northwesterly wind in winter and by easterly wind in summer, but the amplitude of the wind speed in summer was relatively small. We could confirm that these characteristics were consistent at all altitudes and closely correlated with each other by altitude. These characteristics appeared similarly in the diurnal wind speed, and there was generally a 1 h difference among vertical layers. These delays differed according to the season, with spring and fall exhibiting a division at different altitudes showing consistent characteristics, whereas in summer, the maximum wind speed occurred simultaneously 10 h earlier at most altitudes, except for in some of the upper layers. This seems to be due to the relatively strong solar radiation and active vertical mixing. In winter, the maximum wind speed was nonlinear; therefore, the delay characteristics between altitudes did not appear, which was due to influence of strong northwesterly winds, contrary to summer. Additionally, the wind speed exhibited a long-term increasing tendency after decreasing for more than 10 years, which is consistent with previously known research results and the corresponding AWS results.

This study contributes to the field of wind energy and wind measurement campaigns by providing additional information on what altitude is important in monthly and diurnal cycles where the maximum wind occurs and is maintained. And a new finding revealed that the recent increasing tendency of wind speed occurred not only at our research site but also at the AWSs around the site in the five-year analysis. The delayed relationship in the maximum wind speed among altitudes in the diurnal cycle according to different seasons can be useful information for operating wind plants related to the development of wind power generation efficiency. Through this study, it was possible to understand the vertical wind characteristics via intuitive observations using Wind-LIDAR without relying on ground observations based on the similarity theory. In addition, it has been shown that the atmospheric stability has an impact on the vertical wind structure, and it has been related to wind farm performance in several reports [9,11,37–40]. Considering the atmospheric stability and the long-term trend of the vertical wind structure analyzed in this study, more reliable and improved information can be provided. Furthermore, the recent studies on Urban Air Mobility (UAM) report that understanding the vertical wind structure is important for taking off and landing [41,42]. It is expected that the results of this study can be helpful for the safe operation of UAM.

**Author Contributions:** Conceptualization, D.-W.Y. and S.-S.L.; methodology, D.-W.Y., S.-S.L. and H.-W.C.; software, D.-W.Y.; validation, D.-W.Y., S.-S.L. and H.-W.C.; formal analysis, D.-W.Y. and S.-S.L.; investigation, Y.H.L.; resources, D.-W.Y.; data curation, D.-W.Y.; writing—original draft preparation, D.-W.Y.; writing—review and editing, all authors; visualization, D.-W.Y.; supervision, S.-S.L.; project administration, Y.H.L.; funding acquisition, Y.H.L. All authors have read and agreed to the published version of the manuscript.

**Funding:** This research was funded by the Korea Meteorological Administration Research and Development Program “Developing Technology for User-Specific Weather Information” under Grant (KMA2018-00622).

**Institutional Review Board Statement:** Not applicable.

**Informed Consent Statement:** Not applicable.

**Data Availability Statement:** The Wind-LIDAR data were obtained from the National Institute of Meteorological Sciences. The datasets of automatic weather stations (AWSs) used in this study are publicly available in the following archives: <https://data.kma.go.kr> accessed on 1 September 2021.

**Acknowledgments:** We cordially thank the reviewers for their thoughtful comments and constructive suggestions. We also thank Hyeong-Se Jeong for the efforts in managing Wind-LIDAR and maintaining the collection of observation data.

**Conflicts of Interest:** The authors declare no conflict of interest.

## References

1. Rhodes, C.J. The 2015 Paris Climate Change Conference: COP21. *Sci. Prog.* **2016**, *99*, 97–104. [[CrossRef](#)]
2. Macknick, J.; Newmark, R.; Heath, G.; Hallett, K.C. Operational Water Consumption and Withdrawal Factors for Electricity Generating Technologies: A Review of Existing Literature. *Environ. Res. Lett.* **2012**, *7*, 45802. [[CrossRef](#)]
3. Boyle, G. *Renewable Energy*; Oxford University Press: Oxford, UK, 2004.
4. Stull, R.B. *An Introduction to Boundary Layer Meteorology*; Springer Science; Business & Media: London, UK, 1988; Volume 13, p. 187. [[CrossRef](#)]
5. Porté-Agel, F.; Lu, H.; Wu, Y.T. Interaction Between Large Wind Farms and the Atmospheric Boundary Layer. *Proced. Lutam.* **2014**, *10*, 307–318. [[CrossRef](#)]
6. National Academies of Sciences. *Engineering, and Medicine Thriving on Our Changing Planet: A Decadal Strategy for Earth Observation from Space*; National Academies Press: Washington, DC, USA, 2018. [[CrossRef](#)]
7. National Academies of Sciences. *Engineering, and Medicine. The Future of Atmospheric Boundary Layer Observing, Understanding, and Modeling*; Proceedings of a Workshop; National Academies Press: Washington, DC, USA, 2018. [[CrossRef](#)]
8. Goodess, C.M.; Troccoli, A.; Acton, C.; Añel, J.A.; Bett, P.E.; Brayshaw, D.J.; De Felice, M.; Dorling, S.R.; Dubus, L.; Penny, L.; et al. Advancing Climate Services for the European Renewable Energy Sector Through Capacity Building and User Engagement. *Clim. Serv.* **2019**, *16*, 100139. [[CrossRef](#)]
9. St Martin, C.M.; Lundquist, J.K.; Clifton, A.; Poulos, G.S.; Schreck, S.J. Wind Turbine Power Production and Annual Energy Production Depend on Atmospheric Stability and Turbulence. *Wind Energy Sci.* **2016**, *1*, 221–236. [[CrossRef](#)]
10. Doörenkaämper, M.; Tambke, J.; Steinfeld, G.; Heinemann, D.; Kühn, M. Atmospheric Impacts on Power Curves of Multi-Megawatt Offshore Wind Turbines. *J. Phys. Conf. Ser.* **2014**, *555*, 012029. [[CrossRef](#)]
11. Wharton, S.; Lundquist, J.K. Atmospheric Stability Affects Wind Turbine Power Collection. *Environ. Res. Lett.* **2012**, *7*, 014005. [[CrossRef](#)]
12. Antoniou, I.; Pedersen, S.M.; Enevoldsen, P.B. Wind Shear and Uncertainties in Power Curve Measurement and Wind Resources. *Wind Eng.* **2009**, *33*, 449–468. [[CrossRef](#)]
13. Kashani, A.G.; Olsen, M.J.; Parrish, C.E.; Wilson, N. A Review of Lidar Radiometric Processing: From AD HOC Intensity Correction to Rigorous Radiometric Calibration. *Sensors* **2015**, *15*, 28099–28128. [[CrossRef](#)]
14. Emeis, S.; Harris, M.; Banta, R.M. Boundary-layer Anemometry by Optical Remote Sensing for Wind Energy Applications. *Meteorologische* **2007**, *16*, 337–348. [[CrossRef](#)]
15. Weitkamp, C. Lidar Range-Resolved Optical Remote Sensing of the Atmosphere. In *Springer Series in Optical Sciences*; Springer: Singapore, 2005; Volume 102, p. 40. [[CrossRef](#)]
16. Melfi, S.H.; Lawrence, J.D.; McCormick, M.P. Observation of Raman Scattering by Water Vapor in the Atmosphere. *Appl. Phys. Lett.* **1969**, *15*, 295–297. [[CrossRef](#)]
17. Cooney, J.A. Measurements on the Raman Component of Laser Atmospheric Backscatter. *Appl. Phys. Lett.* **1968**, *12*, 40–42. [[CrossRef](#)]
18. Schotland, R.M. Some Observations of the Vertical Profile of Water Vapor by a laser Optical Radar. In Proceedings of the 4th Symposium on Remote Sensing of Environment, Ann Arbor, University of Michigan, Rio de Janeiro, Brazil, 27–31 May 1966; Volume 12–14, pp. 273–283.
19. Smullin, L.D.; Fiocco, G. Optical Echoes from the Moon. *Nature* **1962**, *194*, 1267. [[CrossRef](#)]
20. Woodbury, E.J.; Congleton, R.S.; Morse, J.H.; Stitch, M.L. *Design and Operation of an Experimental Colidar*; IRE WESCON Convention: San Francisco, CA, USA, 1961; Volume 24.
21. Maiman, T.H. Stimulated Optical Radiation in Ruby. *Nature* **1960**, *187*, 493–494. [[CrossRef](#)]
22. Gonzalez-Aparicio, I.; Monforti, F.; Volker, P.; Zucker, A.; Careri, F.; Huld, T.; Badger, J. Simulating European Wind Power Generation Applying Statistical Downscaling to Reanalysis Data. *Appl. Energy* **2017**, *199*, 155–168. [[CrossRef](#)]
23. Liu, Z.; Barlow, J.F.; Chan, P.W.; Fung, J.C.H.; Li, Y.; Ren, C.; Mak, H.W.L.; Ng, E. A Review of Progress and Applications of Pulsed Doppler Wind LiDARs. *Remote Sens.* **2019**, *11*, 2522. [[CrossRef](#)]
24. Fujii, T.; Fukuchi, T. *Laser Remote Sensing*, 1st ed.; CRC Press: Boca Raton, FL, USA, 2005. [[CrossRef](#)]
25. Kim, H.G.; Chyng, C.W.; An, H.J.; Ji, Y.M. Comparative Validation of Windcube LIDAR and Remtech SODAR for Wind Resource Assessment—Remote Sensing Campaign at Pohang Accelerator Laboratory. *J. Korean Sol. Energy Soc.* **2011**, *31*, 63–71. [[CrossRef](#)]
26. Lee, Y.K.; Lee, S.S.; Kim, H.S. Evaluation of wind hazard over Jeju Island. In Proceedings of the 7th Asia-Pacific Conference on Wind Engineering, Taipei, Taiwan, 8–12 November 2009.
27. Korea Meteorological Administration. *Technical Note of Meteorological Observation Standardization Manual (Publication Registration Number: 11-1360000-001611-09)*; Korea Meteorological Administration: Seoul, Republic of Korea, 2019; pp. 53–57.

28. O'Neill, B.C.; Tebaldi, C.; Van Vuuren, D.P.; Eyring, V.; Friedlingstein, P.; Hurtt, G.; Knutti, R.; Kriegler, E.; Lamarque, J.F.; Lowe, J.; et al. The Scenario Model Intercomparison Project (ScenarioMIP) for CMIP6. *Geosci. Model Dev.* **2016**, *9*, 3461–3482. [[CrossRef](#)]
29. Zha, J.; Shen, C.; Zhao, D.; Wu, J.; Fan, W. Slowdown and Reversal of Terrestrial Near-Surface Wind Speed and Its Future Changes over Eastern China. *Environ. Res. Lett.* **2021**, *16*, 034028. [[CrossRef](#)]
30. Shen, C.; Zha, J.; Zhao, D.; Wu, J.; Fan, W.; Yang, M.; Li, Z. Estimating Centennial-Scale Changes in Global Terrestrial Near-Surface Wind Speed Based on CMIP6 GCMs. *Environ. Res. Lett.* **2021**, *16*, 084039. [[CrossRef](#)]
31. Liu, J.; Gao, Z.; Wang, L.; Li, Y.; Gao, C.Y. The Impact of Urbanization on Wind Speed and Surface Aerodynamic Characteristics in Beijing during 1991–2011. *Meteorol. Atmos. Phys.* **2018**, *130*, 311–324. [[CrossRef](#)]
32. Kim, J.C.; Paik, K. Recent Recovery of Surface Wind Speed After Decadal Decrease: A Focus on South Korea. *Clim. Dyn.* **2015**, *45*, 1699–1712. [[CrossRef](#)]
33. Adams, A.S.; Keith, D.W. Are Global Wind Power Resource Estimates Overstated? *Environ. Res. Lett.* **2013**, *8*, 015021. [[CrossRef](#)]
34. Kim, H.G. Preliminary Estimation of Wind Resource Potential in South Korea. *J. Korean Sol. Energy Soc.* **2008**, *28*, 1–12. [[CrossRef](#)]
35. Baidya Roy, S.; Pacala, S.W.; Walko, R.L. Can Large Wind Farms Affect Local Meteorology? *J. Geophys. Res.* **2004**, *109*, D19. [[CrossRef](#)]
36. Keith, D.W.; DeCarolis, J.F.; Denkenberger, D.C.; Lenschow, D.H.; Malyshev, S.L.; Pacala, S.; Rasch, P.J. The Influence of Large-Scale Wind Power on Global Climate. *Proc. Natl. Acad. Sci. USA* **2004**, *101*, 16115–16120. [[CrossRef](#)] [[PubMed](#)]
37. Jeong, H.S.; Kim, Y.H.; Choi, H.W. Characteristics of Wind Environment in Dongbok Bukchon Wind Farm on Jeju. *New Renew. Energy* **2022**, *18*, 1–16. [[CrossRef](#)]
38. Kim, D.Y.; Kim, Y.H.; Kim, J.H.; Kim, B.J. Spatial characteristics of wind energy resources over terrain in Jeju Island. *New Renew. Energy* **2017**, *13*, 13–20. [[CrossRef](#)]
39. Alblas, L.; Bierbooms, W.; Veldkamp, D. Power output of offshore wind farms in relation to atmospheric stability. *J. Phys. Conf. Ser.* **2014**, *555*, 012004. [[CrossRef](#)]
40. Sumner, J.; Masson, C. Influence of atmospheric stability on wind turbine power performance curves. *J. Sol. Energy Eng.* **2006**, *128*, 531–538. [[CrossRef](#)]
41. Steiner, M. Urban Air Mobility: Opportunities for the Weather Community. *Bull. Am. Meteorol. Soc.* **2019**, *100*, 2131–2133. [[CrossRef](#)]
42. Reiche, C.; McGillen, C.; Siegel, J.; Brody, F. Are We Ready to Weather Urban Air Mobility (UAM)? In Proceedings of the 2019 Integrated Communications, Navigation and Surveillance Conference (ICNS), Herndon, VA, USA, 9–11 April 2019; pp. 1–7. [[CrossRef](#)]

**Disclaimer/Publisher's Note:** The statements, opinions and data contained in all publications are solely those of the individual author(s) and contributor(s) and not of MDPI and/or the editor(s). MDPI and/or the editor(s) disclaim responsibility for any injury to people or property resulting from any ideas, methods, instructions or products referred to in the content.